TRANSNAV the International Journal on Marine Navigation and Safety of Sea Transportation
http://www.transnav.eu
Volume 14
Number 2
June 2020
DOI: 10.12716/1001.14.02.28

Study of Inline-slot Ejector Diffuser Under Varying Ambient Conditions: A Passive Infrared Suppression Device for Ships

L. Singh, S.N. Singh & S.S. Sinha
Indian Institute of Technology Delhi, New Delhi, India

ABSTRACT: Passive infrared (IR) suppression device, commonly known as ejector diffuser, is an integral part of the defence system of a ship. The definitive role of passive IR suppressor to counter the IR tracking and locking of the ship has made them indispensable for any combat marine. The gas turbine exhaust gases are the leading heat source on a ship. The exhaust temperature of the gases ranges between 650K-850K. At such temperatures, the ship can be easily detected by the enemy through IR imaging. The role of the ejector diffuser is to (i) lower the gas turbine exhaust gases temperature to the limits (< 450K) such that the IR locking of the marine can be avoided, and (ii) recover static pressure such that the engine performance of the gas turbine is not affected. Ejector diffuser has the ability to entrain ambient air and allow mixing it with the exhaust gases thereby, lowering the temperature of the exhaust gases. However, the mixed exhaust gases temperature depends on the ambient air temperature which under extreme conditions can fluctuate from 273K to 323K. This temperature range can affect the temperature characteristics of an ejector diffuser. The present study undertakes the effect of ambient temperature on the performance of inline-slot ejector diffuser. The ambient temperature (T0) has been varied in the range 273K ≤ T0 ≤ 323K in the step of 10K. It has been found that the mass entrainment increases (≈ 8%) as the ambient temperature decreases. The core temperature at the exit decreases, from 457.58 K to 417.75K, with a decrease in the ambient temperature. However, no significant changes in static pressure recovery.

NOMENCLATURE

RANS	Reynolds-averaged Navier-stokes equation
FANS	Favre-averaged Navier-stokes equation
SST	Shear stress transport
Re_{nz}	Nozzle exit Reynolds number
U_{in}	Nozzle inlet velocity (m/s)
v_i	Velocity components (m/s)
p	Pressure (Pa)
τ_{ij}	Total stress tensor (m^2/s^2)
e_0	Total energy (J/s)
Φ	Cumulative mass entrainment ratio
κ	Local mass entrainment ratio
ψ	Normalized temperature distribution
C_p	Coefficient of static pressure
y^+	Non-dimensional wall distance
ϱ	Density of air (kg/m^3)
μ	Dynamic viscosity (m^2/s)
μ_t	Turbulent viscosity (m^2/s)
λ	Thermal conductivity (W/mK)
λ_t	Turbulent thermal conductivity (W/mK)
k	Turbulent kinetic energy (m^2/s^{-2})
ω	Specific turbulent dissipation rate (s^{-1})
T	Local temperature (K)
T_0	Ambient temperature (K)
T_g	Gas turbine exit temperature (K)

Superscript

$\tilde{}$ Favre-averaged quantity
$\bar{}$ Reynolds-averaged quantity

1 INTRODUCTION

The ship movement, tracking, and missile locking by the enemy is often achieved by the use of infrared scanning. The hot spots present on the ship structure and exhaust gases acts as the source to infrared scanning. Thus, the survivability of ship will depend upon successful dodging the enemy surveillance. This is achieved through the deployment of infrared suppression system (IRSS) which boost the stealth capabilities of a ship. The passive IRSS helps in reducing the exhaust gases temperature such that the IR signatures are curtailed. The passive IRSS device is commonly known as ejector diffuser, and is installed at the downstream of the gas turbine engine [1]. The aim of ejector diffuser is to entrain cold ambient air and mix it with the hot exhaust gases before they are emitted in the environment. Figure 1 shows the schematic of the ejector diffuser along with its components (i) nozzle, (ii) mixing tube, and (iii) slotted diffuser. The popularity and increase use of IR guided missiles over other (acoustics, laser, visual, radar) missiles [2] requires deeper understanding of passive IRSS device under all varying conditions.

Ejector diffuser being used in the combat ships (confidential), little information is available in open literature. Sen [3] conducted study on the conical stepped ejector diffuser and investigated the effect of various geometrical parameters such as length of overlap at step slots, diffuser wall thickness, and inclined slot openings. While the length of overlap does not offer any gain in diffuser performance, increase in wall thickness adversely affects the performance. Singh et al. [4] studied square shaped step ejector diffuser and reported drop in mass entrainment by 26% for wide angle diffuser. In another article [5], effect of number of slots on the performance was reported wherein increase in slot numbers does not offer any gain in mass entrainment although results in marginal increase in static pressure recovery. Chen et al. [6] studied oblong shaped ejector diffuser and observed better performance than conical ejector diffuser under moderate swirl conditions. A concept of inline-slot was introduced by Singh et al. [7] to understand the mass entrainment characteristics of a conical ejector diffuser where better mass entrainment and pressure recovery is achieved.

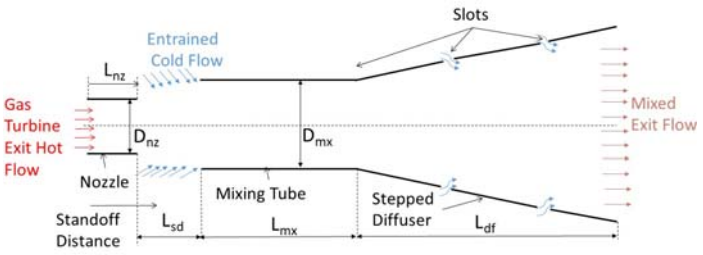

Figure 1. Typical ejector diffuser and its components.

In the present investigation, the effect of ambient temperature on the performance of inline-slot ejector diffuser is studied. As the ambient temperature fluctuates over the year and also with location, the systematic study of the ambient temperature change on the ejector diffuser performance needs to be investigated. Under extreme ambient conditions, the temperature can fluctuate upto 50K. Hence the performance of ejector diffuser under varying ambient temperature is an important study.

2 PROBLEM FORMULATION

The numerical approach has been adopted to study the effect of ambient conditions on the performance of inline-slot ejector diffuser. The gas turbine exhaust gases temperature is fixed at 700K, thus nozzle exit mass flow rate remains same in all the cases. Further, the ambient temperature is varied in the range of $273K \leq T0 \leq 323K$ in steps of 10K. The cases for the present investigation are shown in Table 1.

Table 1. Cases for the current investigation

Case	Ambient Temperature
Case A	273K
Case B	283K
Case C	293K
Case D	303K
Case E	313K
Case F	323K

All other geometric details, boundary conditions, and dynamical parameters between the cases are same.

A two-dimensional axisymmetric domain has been adopted to carry out the numerical study. Figure 2 shows the computational domain, boundary conditions, and the labels for all important dimensions. The labels along with their values are explained in Table 2. The computational domain consists of nozzle, mixing tube, inline-slot diffuser, tailpipe, and the plenum surrounding the ejector diffuser. The dimensions of the plenum, adopted from the literature [6], are sufficiently large so that the imposed boundary conditions at the plenum has minimal interference with the flow characteristics of ejector diffuser. In the present study, the ambient

temperature value is assigned at the plenum boundaries. The other important boundary condition is specified at the inlet of the nozzle, a portion of the left boundary, where a fixed velocity (Re_{nz}=5.0× 10^4) and temperature (700K) are specified. Re_{nz} is calculated for the flow conditions at 700K U_{in}=60m/s, ρ_{in}=0.505kg/m^3, μ_{in}=3.3889552e^{-5} kg/m-s. The boundary conditions at the wall of the ejector diffuser are no-slip for flow variables and thermal coupled wall for the heat transfer variable.

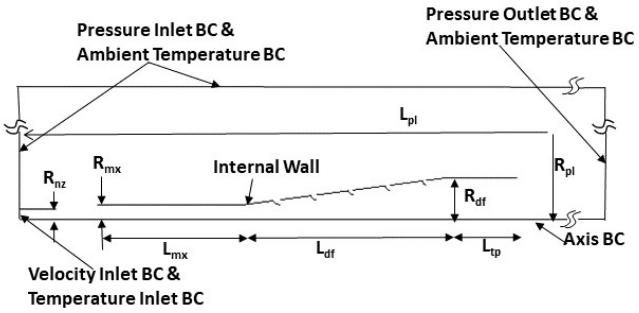

Figure 2. Computational domain and boundary conditions.

Table 2. Dimension of ejector diffuser

Name	Description	Value
D_{nz}	nozzle exit diameter	50mm
L_{nz}	nozzle length	$1D_{nz}$ [4]
L_{sd}	standoff distance	$2.25D_{nz}$ [8]
D_{mx}	mixing tube diameter	$\sqrt{2.25}$ D_{nz} [8]
L_{mx}	mixing tube length	$8D_{nz}$ [8]
L_{df}	length of diffuser	$11D_{nz}$ [3.4]
L_{tp}	length of tail pipe	$4D_{nz}$ [3, 4]
L_{pl}	length of plenum	$65D_{nz}$ [6]
D_{pl}	diameter of plenum	$21D_{nz}$ [6]
AR_{mx}	area ratio of mixing tube inlet to nozzle exit	2.25[8]

The computational domain is discretized using the structured meshing approach where quadrilateral cells are generated to discretize the computational domain. As the present study employs SST k-ω turbulence model, $y^+ \leq 1$ has been maintained to capture the near wall gradients. The grid quality is ensured through the aspect ratio (AS) of each cell. The selection of the grid is decided when the maximum AS ≤ 40.

3 NUMERICAL DETAILS

To conduct the simulation study we used steady state Reynolds averaged Navier-Stokes (RANS) and Favre averaged Navier-Stokes (FANS) equations. An overhead bar represents Reynolds averaged quantity while overhead tilde represents Favre averaged (density weighted averaged) quantity. The set of modelled equations for the current study are given in Eq. (1) to (8):

$$\frac{\partial}{\partial x_i}\left(\bar{\rho}\tilde{v}_i\right) = 0; \tag{1}$$

$$\frac{\partial}{\partial x_j}\left(\bar{\rho}\tilde{v}_j\tilde{v}_i\right) = -\frac{\partial}{\partial x_j}\left(\bar{p}\delta_{ij}\right) + \frac{\partial}{\partial x_j}\left(\tilde{\tau}_{ji}^{tot}\right); \tag{2}$$

$$\frac{\partial}{\partial x_j}\left(\bar{\rho}\tilde{e}_0\right) = \frac{\partial}{\partial x_j}\left(\tilde{q}_j^{tot}\right) + \frac{\partial}{\partial x_j}\left(\tilde{v}_j\bar{p}\right); \tag{3}$$

$$\tilde{\tau}_{ij}^{tot} = \tilde{\tau}_{ij}^{lam} + \tilde{\tau}_{ij}^{turb}; \quad \tilde{q}_j^{tot} = \tilde{q}_j^{lam} + \tilde{q}_j^{turb} \tag{4}$$

$$\tilde{\tau}_{ij}^{lam} = \mu\left[\left(\frac{\partial\tilde{v}_i}{\partial x_j} + \frac{\partial\tilde{v}_j}{\partial x_i}\right) - \frac{2}{3}\frac{\partial\tilde{v}_k}{\partial x_k}\delta_{ij}\right] \tag{5}$$

$$\tilde{\tau}_{ij}^{turb} = \mu_t\left[\left(\frac{\partial\tilde{v}_i}{\partial x_j} + \frac{\partial\tilde{v}_j}{\partial x_i}\right) - \frac{2}{3}\frac{\partial\tilde{v}_k}{\partial x_k}\delta_{ij}\right] - \frac{2}{3}\bar{\rho}k\delta_{ij} \tag{6}$$

$$\tilde{q}_j^{lam} = \lambda\frac{\partial\tilde{T}}{\partial x_j}; \quad \tilde{q}_j^{turb} = \lambda_t\frac{\partial\tilde{T}}{\partial x_j} \tag{7}$$

$$\bar{p} = \bar{\rho}\frac{R}{\gamma}\tilde{T}; \quad \gamma = \frac{c_p}{c_v} \tag{8}$$

Further temperature dependent air properties are adopted for all the cases. The piece-wise polynomial functions for the thermal conductivity (λ), specific heat at constant pressure (c_p), and dynamic viscosity (μ), adopted from [9], are shown below:

$$\lambda = 1.00233\times10^{-3} + 9.04396\times10^{-5}T - 2.90213\times10^{-8}T^2 + 4.63995\times10^{-12}T^3 - 2.16473\times10^{-22}T^4 + 6.96289\times10^{-26}T^5; \tag{9}$$

$$c_p = 9.55481 + 6.29068\times10^{-1}T - 3.10144\times10^{-3}T^2 + 6.92621\times10^{-6}T^3 - 6.37568\times10^{-9}T^4 + 2.10762\times10^{-12}T^5; \tag{10}$$

$$\mu = 2.57183\times10^{-7} + 8.54743\times10^{-8}T - 1.0303\times10^{-10}T^2 + 1.09789\times10^{-13}T^3 - 6.76718\times10^{-17}T^4 + 1.75005\times10^{-20}T^5 \tag{11}$$

In the present study, SST k-ω turbulence model is selected to conduct the numerical study [8]. The complete set of closure equations for SST k-ω can be found in [10]. The validation study is performed by comparing the predicted axial velocity profile with the inhouse experimental measurements on an ejector diffuser at multiple axial locations (see Figure 3). Figure 4 shows the comparison of axial velocity profile at Location AA. Similar axial velocity comparison plots are obtained for other locations. The

numerical axial velocity profile shows reasonable matching with the experimental data points. A maximum of 18% local deviation in the axial velocity is observed at the axis of the ejector diffuser whereas <4% deviation in the mass-weighted average value of the axial velocity is observed.

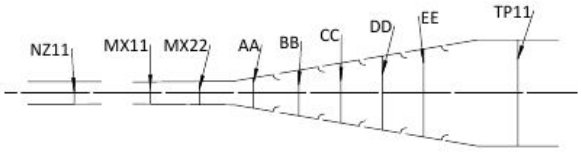

Figure 3. Radial line sections where results are extracted.

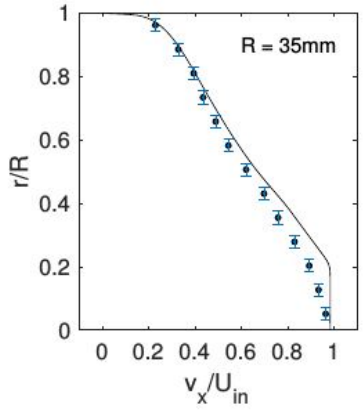

Figure 4. Comparison of experimental and numerical axial velocity profile upstream of first slot.

The mesh independence study and the order of convergence analysis has been conducted for three grids, coarse = 0.5×10^5, medium = 1.0×10^5, fine = 1.8×10^5, with the grid refinement factor of 2. Figure 5 shows the plot of coefficient of static pressure C_p verses the grid index (GI) factor, where $GI=1/N^{[2/2]}$ and N is the total number of cells in a grid [11]. It can be seen that the error between the medium and fine grid is relatively small. Further, the selected order of accuracy (p) for the simulation study is a second-order accurate (p=2) scheme. Figure 5 shows that C_p for the three grids falls on the straight line, thus depicting the order of convergence as a second order accurate solution. For the current study, medium grid is selected for all the simulation.

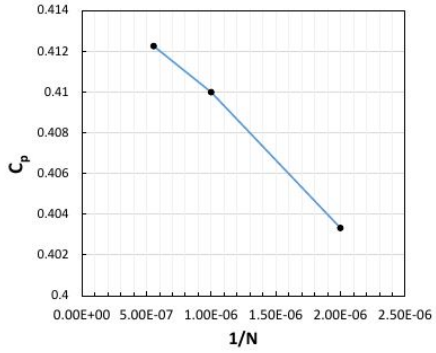

Figure 5. Grid independence and order of convergence analysis as second order scheme.

Governing equations are integrated over the discretized computational domain by finite volume technique (FVM). For better accuracy, a 2nd order upwind scheme is employed to discretize the equations for momentum, k, ω and energy. However, in order to achieve convergence (convergence criteria of 10^{-6}), a 1st order upwind scheme was initially used to obtain the solution. Then this converged solution is used as initial guess to obtain solution for 2nd order upwind scheme. SIMPLE algorithm is used for pressure velocity coupling to solve the pressure correction equation in an iterative method until convergence is achieved.

4 RESULTS AND DISCUSSION

The results are presented in three parts (i) mass entrainment ratio, (ii) thermal characteristics, and (iii) static pressure recovery.

4.1 *Effect of ambient conditions on the local and cumulative mass entrainment ratios*

The amount of mass entrained (ambient air) by an ejector diffuser is an important performance parameter. As there are multiple slots present on the surface of ejector diffuser, mass entrainment is estimated by local mass entrainment ratio (κ) and cumulative mass entrainment ratio (φ). They are defined by Equations 12 and 13:

$$\kappa = \frac{m_{je}}{m_{in}}, \tag{12}$$

$$\phi = \frac{\sum m_{je}}{m_{in}}, \tag{13}$$

where m_{je} represent entrained mass flow rate through an individual slot opening and m_{in} is nozzle exit mass flow rate.

Figure 6 shows the mass entrainment through the individuals' slots. At z/L=0.11 which corresponds to the mass entrainment through the standoff distance (SD), Case A shows the highest entrainment while Case F has the least value. The variation between the maximum to minimum κ at SD is ~8%. This highlights that the ambient temperature affects the mass entrainment through standoff distance. With the increase in ambient temperature the mass entrainment through SD decreases.

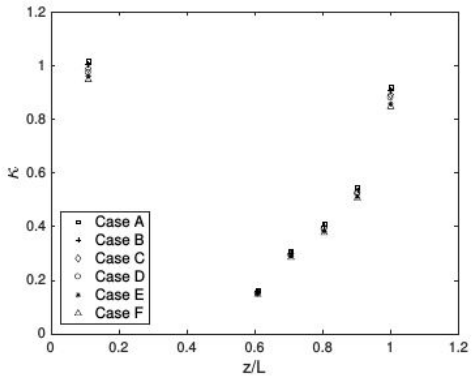

Figure 6. Comparison of κ for all the cases.

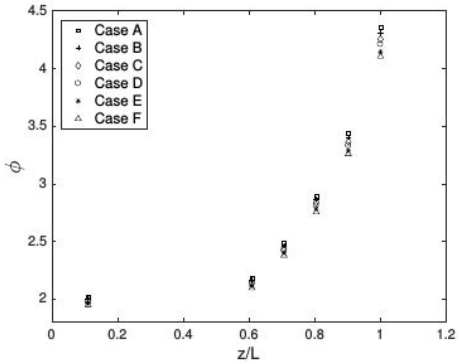

Figure 7. Comparison of φ for all the cases.

For 0.6≤ z/L≤ 1, represent five diffuser slot openings, the values of κ at the first and second slots for all the cases shows no significant variation. Only at the third slot, and onwards the variation in κ between the cases is visible. The difference in κ at the last slot is significant with the variation between the maximum and minimum value being ~ 8%. Thus, the change in ambient temperature also affects the local mass entrainment downstream of the diffuser. The mechanism of mass entrainment takes place due to the pressure differential across an opening, and by momentum exchange between two streams moving at different speeds at the shear layer. However, in the present study the changes in the flow field is primarily governed by the change in the air properties as a function of temperature. Figure 8 shows the comparison of density field for Case A and Case F. It can be seen that entrained air in Case F is less dense which in turn affects the density field inside the diffuser. This will lead to variation in the mass entrainment characteristics. The analysis of cumulative mass entrainment ratio (φ) reveals that maximum φ=4.36 is achieved for Case A and it tends to reduce with increase in ambient temperature.

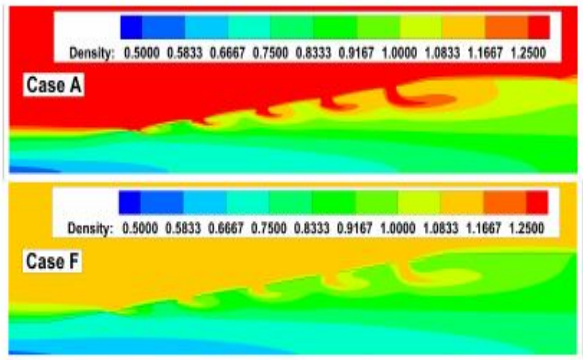

Figure 8. Comparison of density field in Case A and Case F.

4.2 *Effect of ambient conditions on temperature distribution*

To understand the distribution of infrared energy from the exhaust gases, we plot normalized temperature variation (ψ) parameter which will reveal extent of cooling at a given location of interest. It is defined as (Equation 14):

$$\psi = \frac{T - T_0}{T_g - T_0}, \tag{14}$$

where T is the local temperature, T_0 is the ambient temperature and T_g is the temperature of exhaust gas at the nozzle exit. The most important locations are ejector diffuser exit and its walls. Further local thermal mixing profiles are useful to understand the local mixing capabilities of an ejector diffuser exit for all the cases. It can be seen that the shape of the thermal profiles is very similar for all the cases. All profiles tend to merge for the large part of the radial distance. Only at the core, significant variations tend to exits. Case A has a minimum temperature with $\psi = 0.339$ (T=417.75K), which are within the limits, at the core while Case F has higher value $\psi = 0.357$ (T=457.58K). The difference can be attributed to higher mass entrainment in Case A. Further, ψ is plotted at the wall of the ejector diffuser with no significant changes are observed between the cases. It shows that the effect of ambient temperature is more dominant at the core of the ejector diffuser while at other locations the effect is minimal.

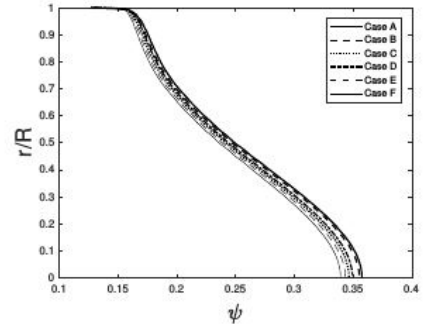

Figure 9. Normalized temperature variation at ejector diffuser exit.

4.3 *Effect of ambient conditions on static pressure recovery*

Static pressure recovery is defined in terms of coefficient of pressure recovery (C_p). In the case of mass entraining ejector diffusers, C_p is defined as [12]:

$$C_p = \frac{\left(p_{ex} - p_{in}\right)\left(m_{in} + \Sigma m_{je}\right)}{\frac{1}{2}\left(\rho_{in} U_{in}^2 m_{in}\right)}, \quad (15)$$

where p_{ex}, p_{in} are the mass-weighted static pressure at the diffuser exit and reference location (mixing tube location), ρ_{in}, U_{in} are density and axial velocity at mixing tube inlet. Figure 10 shows the plot of C_p verses non-dimensional length (z/L). It can be seen that the static pressure recovery profiles for all the cases overlaps which indicates no effect of ambient temperature on the pressure recovery.

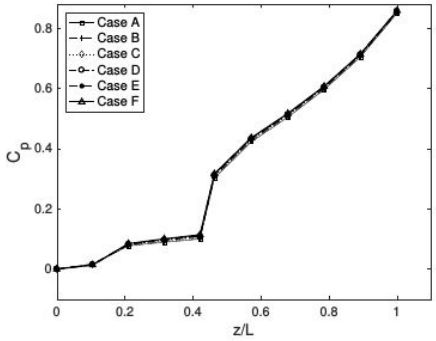

Figure 10. Comparison of static pressure recovery for all the cases.

5 CONCLUSIONS

A numerical study has been performed on a inline-slot ejector diffuser wherein the effect of ambient temperature is investigated using SST k-ω turbulence model. Ambient temperature is systematically varied in the range 273K≤ T_0 ≤ 323K in the step of 10K while keeping other geometrical parameters same for all the cases. Boundary conditions and dynamical parameters remain consistent for all the simulations. Performance for all the cases has been compared in terms of mass entrainment, thermal profiles, and static pressure recovery. It has been found that with the increase in ambient temperature, the mass entrainment decreases. The variation upto 8% in the local as well as cumulative mass entrainment ratios are observed for the ambient temperature range investigated. The core temperature at the ejector diffuser exit decreases, from 457.58K to 417.75K, with decrease in the ambient temperature while no other significant changes in the thermal characteristics are observed. The static pressure recovery does not depend on the ambient conditions at all since the profiles for all the cases matches with each other. Thus, the current study reveals that the change in ambient temperature up to 50K will affect mass entrainment and core temperature while there will be no effect on static pressure recovery.

REFERENCES

[1] AM Birk and D VanDam. Marine gas turbine infrared signature suppression: Aerothermal design considerations. International Gas Turbine and Aeroengine Congress and Exposition, pages V002T03A009–V002T03A009–10, 1989.

[2] Arvind Gangoli Rao. Infrared Signature Modeling and Analysis of Aircraft Plume. International Journal of Turbo and Jet Engines, 28:187, 2011.

[3] Saibal Sen. Studies on Flow Characteristics of a Stepped Conical Diffuser with Passive Suction. PhD thesis, Department of Applied Mechanics, Indian Institute of Technology Delhi, 2008.

[4] Parminder Singh, S N Singh, and V Seshadri. Experimental Investigations on Non-Circular Ejector Air Diffusers. 39th AIAA Fluid Dynamics Conference, page 4213, 2009.

[5] Parminder Singh, Sidh Nath Singh, and V Seshadri. Effect of number of slots and overlap on the performance of non-circular ejector air diffuser. In 43rd AIAA Fluid Dynamics Conference, page 2729, 2013.

[6] Qi Chen. Performance of air-air ejectors with multi-ring entraining diffusers. PhD thesis, Department of Mechanical and Materials Engineering, Queen's University, 2008.

[7] L Singh, SN Singh, and SS Sinha. Effect of slot-guidance and slot-area on air entrainment in a conical ejector diffuser for infrared suppression. Journal of Applied Fluid Mechanics, 12(4):1303–1318, 2019.

[8] L Singh, SN Singh, and SS Sinha. Effect of standoff distance and area ratio on the performance of circular exhaust ejector using computational fluid dynamics. Proc. IMechE, Part G: Journal of Aerospace Engineering, 232(15):2821–2832, 2018.

[9] A Maqsood. A study of subsonic air-air ejector with short bent mixing tube. PhD thesis, Department of Mechanical and Materials Engineering, Queen's University at Kingston, Canada, 2008.

[10] Florian R Menter. Two-equation eddy- viscosity turbulence models for engineering applications. Journal of AIAA, 32(8):1598-1605, 1994.

[11] Simone Crippa. Improvement of unstructured computational fluid dynamics simulations through novel mesh generation methodologies. Journal of Aircraft, 48(3):1036–1044, 2011.

[12] W. B. Nicoll and B. R. Ramaprian. Performance of conical diffusers with annular injection at inlet. Journal of Fluids Engineering, 92(4):827–835, 1970.